International Journal of Microwave and Wireless Technologies

cambridge.org/mrf

New method based on genetic algorithm and Minkowski fractal for multiband antenna designs

Bouchra Ezzahry, Taj-Eddin Elhamadi, Mohammed Lamsalli and Naima Amar Touhami

Electronic & Smart Systems (ESS) Team, Intelligent Systems Design (ISD) laboratory, Faculty of Sciences, Abdelmalek Essaadi University, Tetouan, Morocco

Research Paper

Cite this article: Ezzahry B, Elhamadi TE, Lamsalli M, Touhami NA (2024) New method based on genetic algorithm and Minkowski fractal for multiband antenna designs. *International Journal of Microwave and Wireless Technologies* **16**(3), 466–477. https://doi.org/10.1017/S1759078723001071

Received: 21 March 2023
Revised: 31 August 2023
Accepted: 05 September 2023

Keywords:
CST-API; compact; 5 GHz WLAN band; genetic algorithm; Matlab; Minkowski island fractal; multiband antenna; multi-objective; parallel computing; Roulette Wheel selection

Corresponding author: Bouchra Ezzahry; Email: ezzahrybouchra@gmail.com

Abstract

In this paper, a new method based on a genetic algorithm and Minkowski Island fractal is proposed for multiband antennas. Three-antenna configurations are chosen to validate the proposed optimization procedure. The first configuration is a wide-band antenna, operating in the WLAN (wireless local area network) UNII-2C band. The second configuration is a dual-band antenna, operating in the WLAN UNII-2 and UNII-2C bands. In contrast, the third is a tri-band antenna operating in the UNII-2, UNII-2C, and UNII-3 bands. The optimization process is accelerated by using the Computer Simulation Technology (CST) Application Programming Interface which allows all genetic operators to be performed in MATLAB while the numerical calculations are running in the internal CST Finite-Difference Time-Domain -solver using parallel computing with GPU acceleration. All three designed configurations are manufactured using a 0.8 mm thick FR4 epoxy substrate with a relative dielectric constant of 4.8. The return loss and the radiation pattern's measurements agree well with the simulation results. Further, the methodology presented can be very effective in terms of size reduction; the designed antennas are $24 \times 24 \times 0.8$ mm^3 (460 mm^3).

Introduction

Multiband antennas are designed to operate over a wide range of frequencies. They are often used in applications where it is necessary to communicate on several frequency bands, such as in a cellular or satellite mobile communication system. Multiband antennas also allow the communication system to support various standards, which can differ from country to country.

Many microstrip and coplanar waveguide multiband antennas are developed in the literature to include different standards in one patch. Some antennas are designed to include both 2.4 and 5 GHz WLAN (wireless local area network) and WiMAX (Worldwide Interoperability for Microwave Access) communications [1]. Some have been specially designed for mobile devices to support GSM (Global System for Mobile Communications), LTE (Long-Term Evolution), and UMTS (Universal Mobile Telecommunications System) cellular protocols in addition to WLAN/WiMAX bands [2]. We can also develop others for Internet of Things (IoT) applications, including WLAN, WiMAX, and C-band communications [3].

Multiband antennas can be designed using many different techniques [4]. The multilayer PIFA (planar inverted-F antenna) configuration is often used for cellular mobiles to achieve multiband operation in the ISM (Industrial, Scientific, and Medical) band [5]. Another promising technique is based on the use of frequency selective surface to provide selectivity in the frequency response of the antenna [6]. We can also mention the metamaterials, which can be used for this purpose [7, 8].

Another alternative that has caught the attention of researchers is that based on fractal geometries because of its self-similarity and space-filling properties [9]. Self-similarity is to multiplying the copies of the original shape with different scaling factors and space-filling consists of diminishing the antenna size. Concerning this fractal technique, the antenna can operate on multiple frequencies by resolving the spacing problem [10]. Many articles have been published in this context. In paper [11], the tree-like fractal structure is used for a dual-band microstrip RFID (radio Frequency identification) antenna. In [12] Koch curve fractal is used for IoT (radio frequency identification) applications, while the Minkowski fractal is used in paper [13] for WLAN/WiMAX communications. We can also cite the Hilbert curve fractal employed in paper [14] for designing a dual-band RFID tag antenna for high frequency and ultra-high frequency applications. Further, the Koch snowflake fractal

https://doi.org/10.1017/S1759078723001071 Published online by Cambridge University Press

is employed in paper [15] for a planar multiband antenna for cognitive radio.

In this work, we propose to design multiband antennas for 5 GHz WLAN communications. The full 5 GHz WLAN range covers frequencies from 5.15 to 5.85 GHz. It can be used in IEEE 802.11 a & n. The 5 GHz WLAN band is divided into three sub-bands named respectively UNII-1, UNII-2A, UNII-2C, and UNII-3, and the future bands UNII-2B and UNII-4 [16]. The 5 GHz band offers significantly more bandwidth than the 2.4 GHz band. All 5 GHz channels offered, support a channel width of at least 20 MHz without overlap and it can achieve 160 MHz of width.

To meet these specifications, Minkowski fractal geometries are combined with genetic algorithms (GAs). The Minkowski iteration will be used as chromosomes, resulting in a non-uniform fractal antenna, and allowing control over the allowed bands. For the Minkowski Island fractal, the initiator is a Euclidean square.

A GA is a heuristic optimization method inspired by the process of natural selection in biology [17]. A set of individuals, also called an initial population, is built from the chains of chromosomes or genes, coded in binary (0 and 1). The GA then uses different operators, such as selection, crossing, and mutation to evolve the population of individuals over several generations until convergence toward the optimal individual carrying the chromosomes/genes meeting the optimization goals. In recent years, the GA has become a very powerful optimizing tool in the field of antenna design [18]. Questions of miniaturization [19] and improved gain [20] were explored using this technique, in addition to addressing the challenges associated with optimizing multiband antennas [21, 22].

For the present optimization problem, the chromosomes will be the three-iteration Minkowski fractal generators. The GA will generate an initial population of antennas by a random set of chromosomes. This process will provide a wide range of possible configurations, unlike a standard fractal antenna, allowing for greater diversity and increasing the likelihood of having multiband antennas on the desired bands. The resulting antennas are therefore non-uniform fractals, three Minkowski generators coexist in the same individual.

To apply the GA operators, we will need to evaluate the individuals (antennas) at each generation. To meet this requirement, CST's (Computer Simulation Technology) internal FDTD (Finite-Difference Time-Domain)-solver is used and automated from MATLAB. This process can take hours or even days if we evaluate one antenna at a time. To reduce the convergence time, parallel computing is highly essential [23]. Additionally, GPU (Graphics Processing Unit)-based acceleration is used in CST to further speed up the numerical method [24].

This article will be organized as follows: in the "Methods" section, the design step will be exposed first, followed by the overall optimization procedure and the description of the main GA operators, namely selection, crossing, and mutation. In the "Results and discussion" section, the three antennas designed and prototyped to validate the proposed optimization procedure are presented, while specifying the choices of the fitness function and the GA parameters set for each example. The results obtained in terms of return losses and radiation patterns are then presented and discussed.

Methods

Antenna design

The started antenna illustrated in Fig. 1 is a simple square microstrip patch. The antenna is fed by a 50 Ω coax probe.

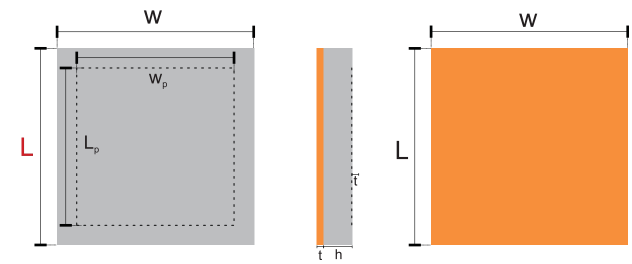

Figure 1. Started antenna structure. (a) Top view, (b) Side view, (c) Bottom view.

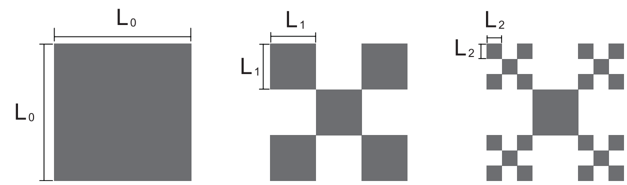

Figure 2. First three iterations of Minkowski Island fractal generation.

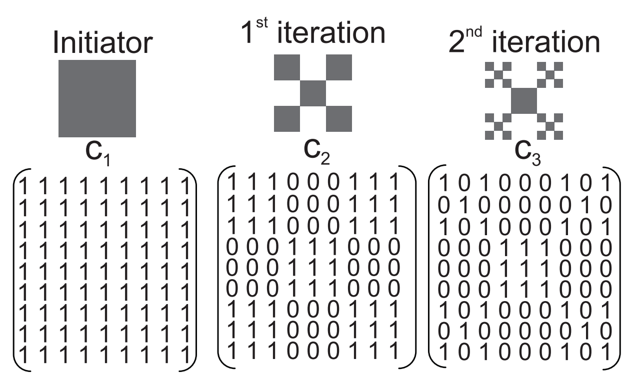

Figure 3. Generation procedure of a Minkowski fractal with the corresponding binary arrays.

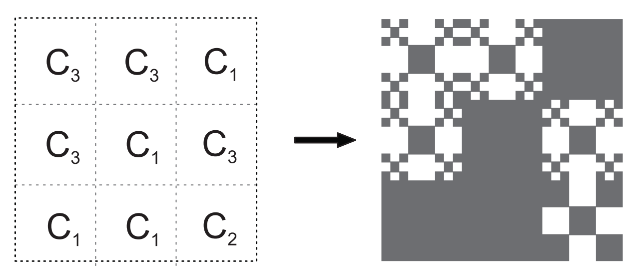

Figure 4. Example of a possible antenna configuration based on the three chromosomes.

The radiating element of the patch antenna is constructed by splitting a square patch into nine elements known as chromosomes. There are three types of chromosomes noted C_1, C_2, and C_3 which represent, respectively, the initiator, the first and the second iterations of the Minkowski Island fractal. The process of generating the first three iterations is shown in Fig. 2 [25]. Equation (1) gives the square dimension at the n^{th} iteration.

$$L_n = \left(\frac{1}{3}\right)^n \times L_0 \tag{1}$$

Figure 3 shows how to generate a Minkowski fractal with the corresponding binary arrays. An example of a possible antenna

https://doi.org/10.1017/S1759078723001071 Published online by Cambridge University Press

Table 1. Summary of genetic algorithm vocabulary and its match for antenna design

Genetic vocabulary	Description	Illustration
Gene	Elementary element to build a chromosome	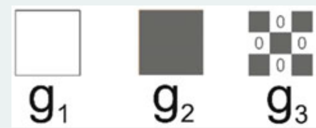
Chromosome	Set of genes with respect to the Minkowski iterations	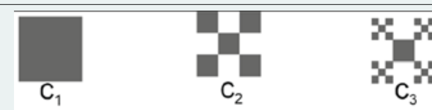
Individual	Set of chromosomes representing a patch antenna	
Population	Group of individuals (antennas)	

configuration based on the three chromosomes is shown in Fig. 4. The Minkowski initiator (chromosome C_1) is a $L_0 = L_p/3$ side square, while the dimension of C_2 and C_3 chromosomes are obtained by applying equation (1) mentioned in the introduction section. For C_2, each element is a $L_p/3$ side square, while for C_3 the smallest element is a $L_0/9$ side square.

The coaxial fed position is chosen randomly, making sure that the chosen position matches well with a type C_1 chromosome to ensure electrical contact.

To respect the vocabulary of the GA, we can also define what we call in GA the genes which indeed represent the bricks with which we could build the chromosomes. Table 1 summarized the GA vocabulary and its match for antenna design.

Figure 5 shows how electrical contact can be ensured by adding overlaps at the corners between two cells (bits). The width of the overlaps is adjusted in a way that does not influence the response of the original antenna. This is also limited by the precision of the manufacturing machine. For this design, the width of the overlaps is fixed at 0.1 mm.

GA-based optimization procedure

The optimization process is mainly executed in the MATLAB environment. The numerical analysis is automated using the FDTD-based internal solver of CST Microwave Studio. Using a parallel calculation, a lot (batch) of antennas can be analyzed simultaneously. Each antenna is assigned to one of the CPU (central processing unit) workers dedicated to this issue. The GA-based optimization procedure will take the following steps (see Fig. 6):

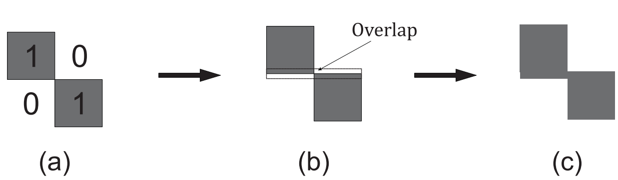

Figure 5. Overlaps added to ensure electrical contact.

- **Step 1**: Initial population generation

An initial population generation is based on a random set of chromosomes. The C_1 chromosome type is imposed on the center of all individuals (see Fig. 4).

- **Step 2**: Numerical analysis of individuals using parallel computing in CST.

The population set of individuals (antennas) is designed and analyzed by using the FDTD-based internal solver of CST Microwave Studio. Each antenna (individual) is assigned to one of the CPU cores (worker). If the number of individuals exceeds the max CPU cores, the population is divided into several batches.

- **Step 3**: Data export:

The S-parameters resulting from the CST analysis are exported to MATLAB for further operation of the GA.

- **Step 4**: Fitness function Evaluation.

The fitness function (F) is given for this multi-objective optimization problem as follows:

$$F = \sum_{1}^{M} \alpha_i \left[\frac{1}{N} \sum^{f_k} \left| S_{11}^{k}\,(dB) \right| \right] \tag{2}$$

where M represents the frequency operating band number, N represent the sample number, and α_i is a ponderation weight for multi-objective optimization control verifying:

$0 < \alpha_i < 1$ and $\sum_{1}^{N} \alpha_i = 1$

If the convergence criteria are reached, End. Otherwise, go to step 5.

- **Step 5**: New population generation (Offspring)
- The genetic operators of reproduction, namely selection, crossover, and mutation are then applied to obtain a new generation of individuals. The coaxial fed positions are updated at this stage using real crossover operation.

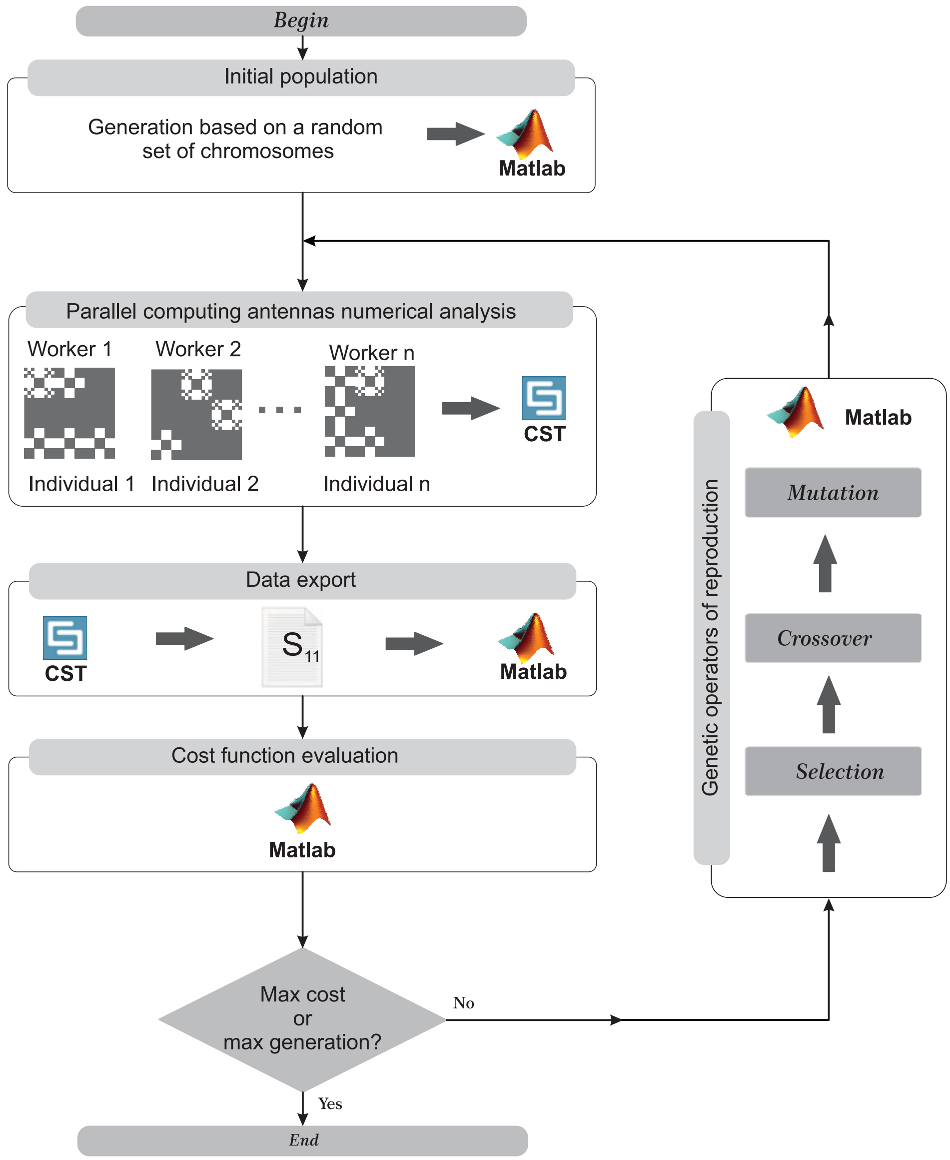

Figure 6. GA-based optimization flowchart.

- Go to **step 2**

GA operators

Selection operator

At this stage, two parents are selected from a set of individuals using the roulette selection method. The selection rate is set at 0.33 (33% of the population). The selection of parents is redone as many times as the size of the population to generate all the offspring's using different parents for each offspring. Figure 7 shows the Roulette Wheel selection principle, while the pseudo-code is given below:

Pseudo-code of the Roulette Wheel selection

$x_i = i^{th}$ individual of the population, $i \in [1, N]$
$f_i \leftarrow$ fitness (x_i) pouri $\in [1, N]$;
$f_{\mathrm{sum}} = \sum_{i=1}^{N} f_i$;
Generate a random number with a uniform distribution $r \in [1, f_{\mathrm{sum}}]$;
$F \leftarrow f_i$;
$k \leftarrow 1$;
As long $F < r$ do
$k \leftarrow k + 1$;
$F \leftarrow F + f_k$;
Selected individual $\leftarrow x_k$;

Crossover operator

The crossover operator is used to generate a new individual (offspring) from two selected parents. The new individual is obtained by random selection of chromosomes alternately among the two

https://doi.org/10.1017/S1759078723001071 Published online by Cambridge University Press

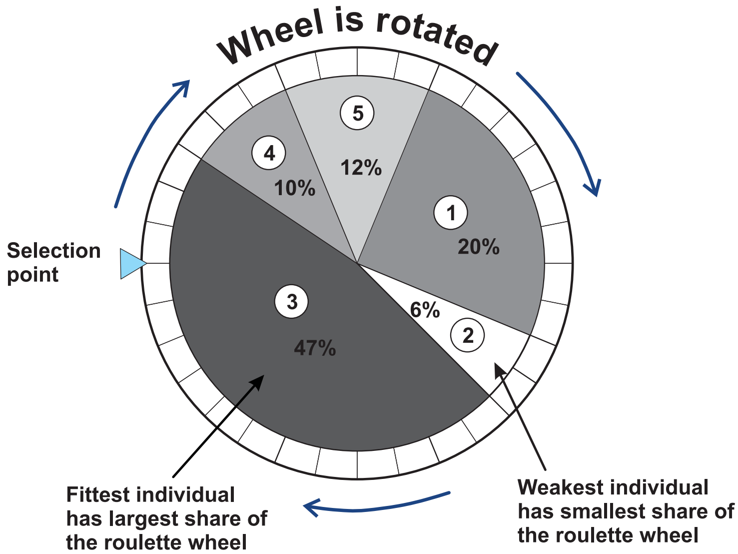

Figure 7. Roulette wheel selection.

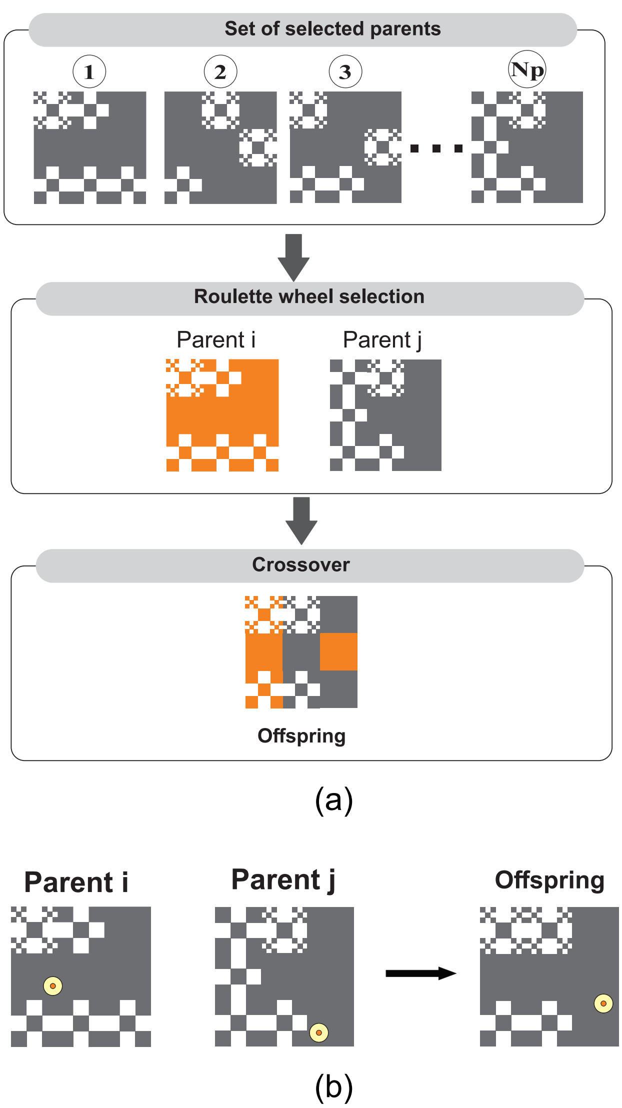

Figure 8. (a) Offspring generation by applying the crossover operator. (b) Example of coaxial fed position crossover.

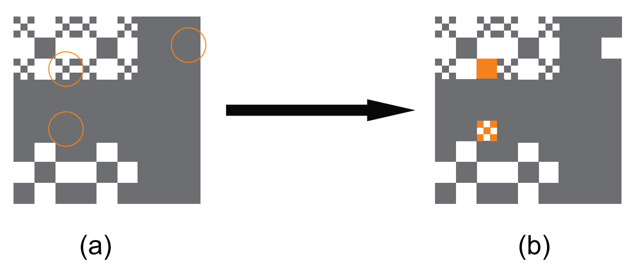

Figure 9. Mutation operation.

parents (uniform crossing). Figure 8a shows the generation of an offspring by applying the crossover operator.

The crossover operator is also used to generate the new coaxial fed positions for the newly generated individuals. The new position is obtained as a linear combination of the parent positions as shown in the following equation:

$$x_{\text{Offspring}} = \alpha . x_{\text{parent1}} + (1 - \alpha) . x_{\text{parent2}} \tag{3–a}$$

$$y_{\text{Offspring}} = \beta . y_{\text{parent1}} + (1 - \beta) . y_{\text{parent2}} \tag{3–b}$$

α, β are real numbers between 0 and 1 randomly generated until the new position matches a metallic area on the patch to ensure electrical contact on the top side. An example is shown in Fig. 8b.

Mutation operator

This operator is usually used optionally to introduce a small change or perturbation in the population with a very low probability. For the current problem 1–5% of the total genes. With individuals having 81 genes, the mutation operation can be applied to 3 randomly selected genes. Figure 9 shows an example of a mutation operation.

Results and discussion

Fitness functions definition

The optimization process detailed in the previous section will be applied to design antennas for the WIFI-IEEE-802.11a standard, known also as WiFi 5 (wireless networking technology). This standard provides high-through put WLANs on the 5 GHz band.

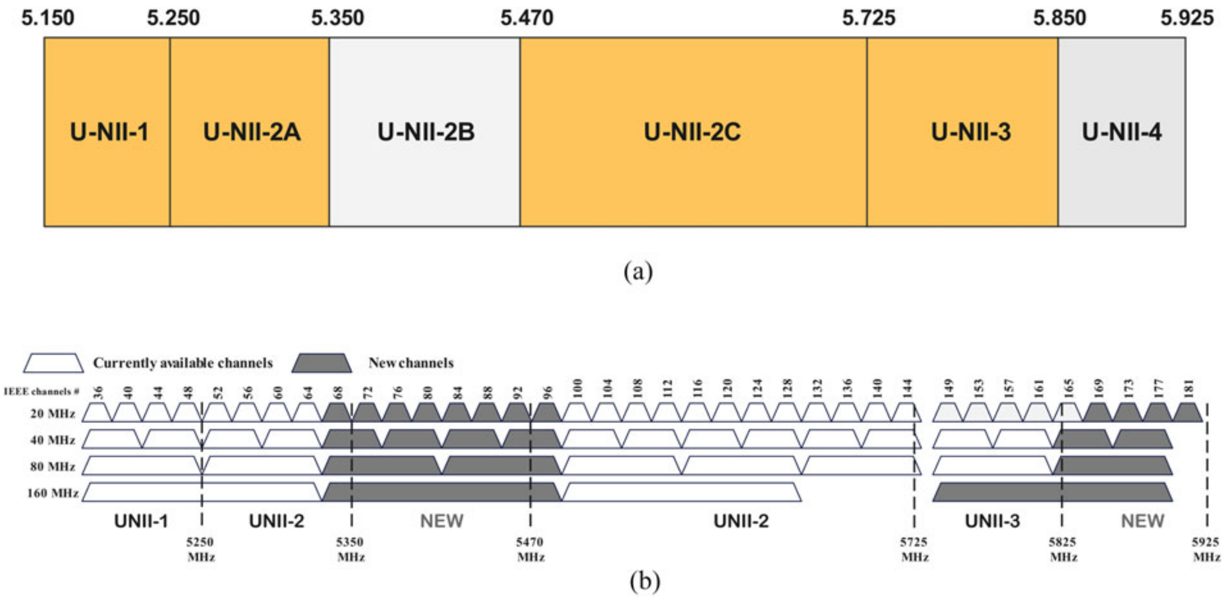

Figure 10. (a) 5 GHz bandplan. (b) Current and proposed 5 GHz channels.

Table 2. Structure parameters

Parameter	Value (mm)	Description
W	30	Substrate width
L	30	Substrate length
w_p	24	Patch width
l_p	24	Patch length

The 5 GHz WLAN band is divided into three sub-bands named respectively UNII-1, UNII-2A, UNII-2C, and UNII-3, in addition to the future bands UNII-2B and UNII-4 as shown in Fig. 10a [16]. The 5 GHz band offers significantly more bandwidth than the 2.4 GHz band. All 5 GHz channels offered, support a channel width of at least 20 MHz without overlap and it can achieve 160 MHz of width (Fig. 10b).

Three different configurations will be tested to validate the efficiency and power of the proposed process optimization algorithm. Therefore, the design of a wide-band, dual-band, and tri-band antenna will be discussed in detail.

The starting antenna selected for this optimization problem is a simple square patch microstrip antenna of 24×24 mm^2 printed on a 30×30 mm^2 FR4 epoxy substrate with a relative dielectric constant of 4.8 The antenna is fed by a 50 Ω coax probe. The started antenna parameters are summarized in Table 2.

The usable frequencies in the IEEE (Institute of Electrical and Electronics Engineers) 802.11a standards occupy 2 wide sub-bands ranging respectively from 5.150 to 5.350 GHz and from 5.470 to 5.850 GHz.

The first antenna will be designed as a wide band to cover the UNII-2C ranging from 5.470 to 5.725 GHz. Thus, it will cover 12 channels from 100 to 144. The optimization problem is a mono-objective, and it can be expressed by:

$$F = \frac{1}{N}\sum^{f_k} \left|S_{11}^{k}\,(dB)\right| \tag{4}$$

where N represents the number of simple frequencies f_k satisfying 5.470 GHz $< f_k <$ 5.725 GHz.

Table 3. GA parameters set

	Values		
Parameters	First antenna	Second antenna	Third antenna
Type	Wide band	Narrow bi-band	Narrow thri-band
Population size	16	24	24
Selection method	Roulette wheel		
Crossover type	Multipoints		
Crossover probability	1/2	2/3	2/3
Mutation probability	No (0 %)		
Generations	10	15	25
Batch (parallel computing)	8		

While the second antenna is a narrow bi-band which will be designed to cover the UNII-2A band ranging from 5.250 to 5.350 GHz (4 channels from 52 to 64), and a part of the UNII-2C band ranging from 5.470 to 5.725 GHz. The optimization problem is a double-objective, and it can be expressed as follows

$$F = \frac{\alpha_1}{N_1}\sum^{f_k} \left|S_{11}^{k}\,(dB)\right| + \frac{\alpha_2}{N_2}\sum^{f_k} \left|S_{11}^{k}\,(dB)\right| \tag{5}$$

where N_1 represents the number of simple frequencies f_k satisfying 5.250 GHz $< f_k <$ 5.350 GHz

N_2 represents the number of simple frequencies f_k satisfying 5.470 GHz $< f_k <$ 5.725 GHz

The ponderation weights are fixed as follows: $\alpha_1 = \alpha_2 = 0.5$.

For the third antenna will be designed as a narrow tri-band to cover the UNII-2A, a part of the UNII-2C, and the UNII-3 bands

Table 4. Average time required for individuals evaluating and for convergence

	Individual evaluating time	One generation evaluation time (with 16 individuals)	Convergence time (10 generations)	Time reduction rate
No parallel calculation	8 min	128 min	1280 min	
8 Parallel workers	10 min	20 min	200 min	6.4 times faster
With CST GPU accelerator	7 min	14 min	140 min	9 times faster

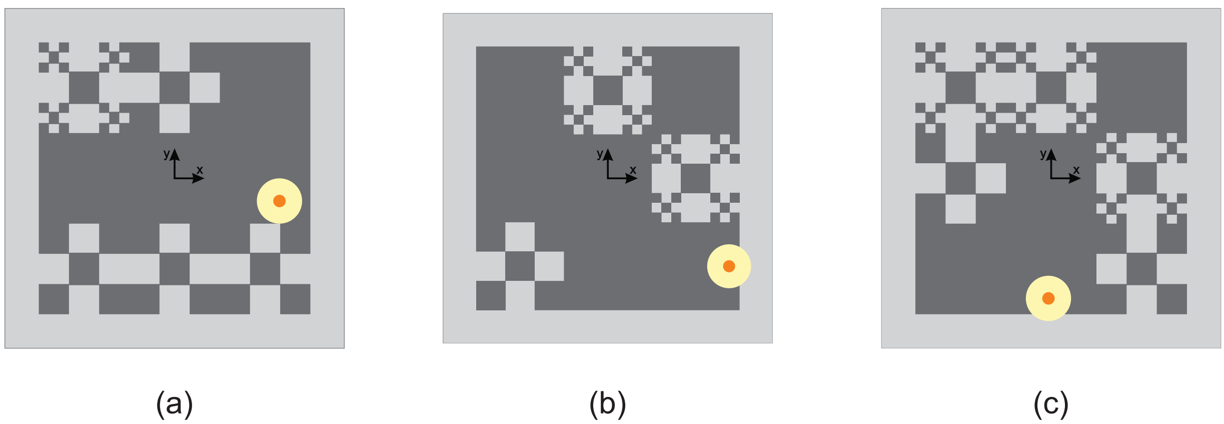

Figure 11. Geometry of the three designed antenna. (a) First, (b) second, (c) and third antenna.

ranging from 5.725 to 5.835 GHz. The optimization problem is a multiobjective, and it can be expressed as follows:

$$F = \frac{\alpha_1}{N_1}\sum^{f_k}\left|S_{11}^k\,(dB)\right| + \frac{\alpha_2}{N_2}\sum^{f_k}\left|S_{11}^k\,(dB)\right| + \frac{\alpha_3}{N_3}\sum^{f_k}\left|S_{11}^k\,(dB)\right| \tag{6}$$

where N_1 represents the number of simple frequencies f_k satisfying 5.250 GHz $< f_k <$ 5.350 GHz

N_2 represents the number of simple frequencies f_k satisfying 5.470 GHz $< f_k <$ 5.7250 GHz

N_3 represents the number of simple frequencies f_k satisfying 5.7250 GHz $< f_k <$ 5.835 GHz

The ponderation weights are fixed as follows: $\alpha_1 = \alpha_2 = \alpha_3 = 0.33$.

GA parameters

The optimization procedure convergence is controlled by several parameters, namely, the size of the initial population, the selection method, the crossover type, as well of the probabilities of crossover and mutation. The GA parameters used for each antenna are summarized in Table 3. Normally, the complexity increases with multi-objective optimization problems. Therefore, the size of the initial population increases from 16 to 24 for antennas 2 and 3. More generations will be necessary for multi-objective optimization problems.

The optimization processes were run on a 2.10 GHz Intel Xeon E5-2620 processor with 8 cores (16 threads) and 32 GB of RAM. This configuration makes it possible to evaluate 8 individuals (batch =8) in parallel by attaching the CST FDTD solver to the eight workers (cores). Additionally, the numerical computation in CST is accelerated by using an NVIDIA Quadro K2200 GPU. Table 4 shows the average time required for individuals evaluating and for convergence, as well as the reduction rate obtained by parallel computing and GPU acceleration.

Experimental results

The optimized antennas shown in Fig. 11 were made using a ProtoMat LPKF S63 rapid printed circuit board prototyping machine. The prototypes are shown in Fig. 12a and b. The prototypes are characterized by their reflection coefficients, which are made by using the Rohde & Schwarz ZVB20 vector network analyzer. Figure 13 shows the measured reflection coefficients $S_{11}\,(dB)$ respectively of the wide-band antenna, the bi-band, and the tri-band antennas. The measured reflection coefficients are compared to the results obtained by electromagnetic (EM) simulation in the CST environment. A good match is observed.

Table 5 summarizes the operating band of the designed antennas concerning the objectives (targets) defined during the GA-based optimization. The first antenna occupies a wide band ranging from 5.49 to 5.78 GHz. Therefore, it allows occupancy of 92% of the UNII-2C band with 11 channels. The second antenna is a dual-band antenna. It allows 53% occupancy of the UNII-2C band with 11 channels with 7 channels and 80% of the UNII-2A band with 3 channels. While the third is a tri-band antenna. It allows 80% occupancy of the UNII-2A band with 3 channels, 47% of the UNII-2C band with 6 channels, and 100% of the UNII-3 band with 5 channels. Table 5 summarizes the realized band and occupied channels for the three designed antennas.

In addition, and to obtain the 2D radiation pattern figure of the realized antennas, we opt for the "Antenna Measurement Systems" from Geozondas Ltd which allows it possible to measure 2D radiation pattern over a wide range of frequencies ranging from 0.1 to 40 GHz. The measurements are made in the pulsed

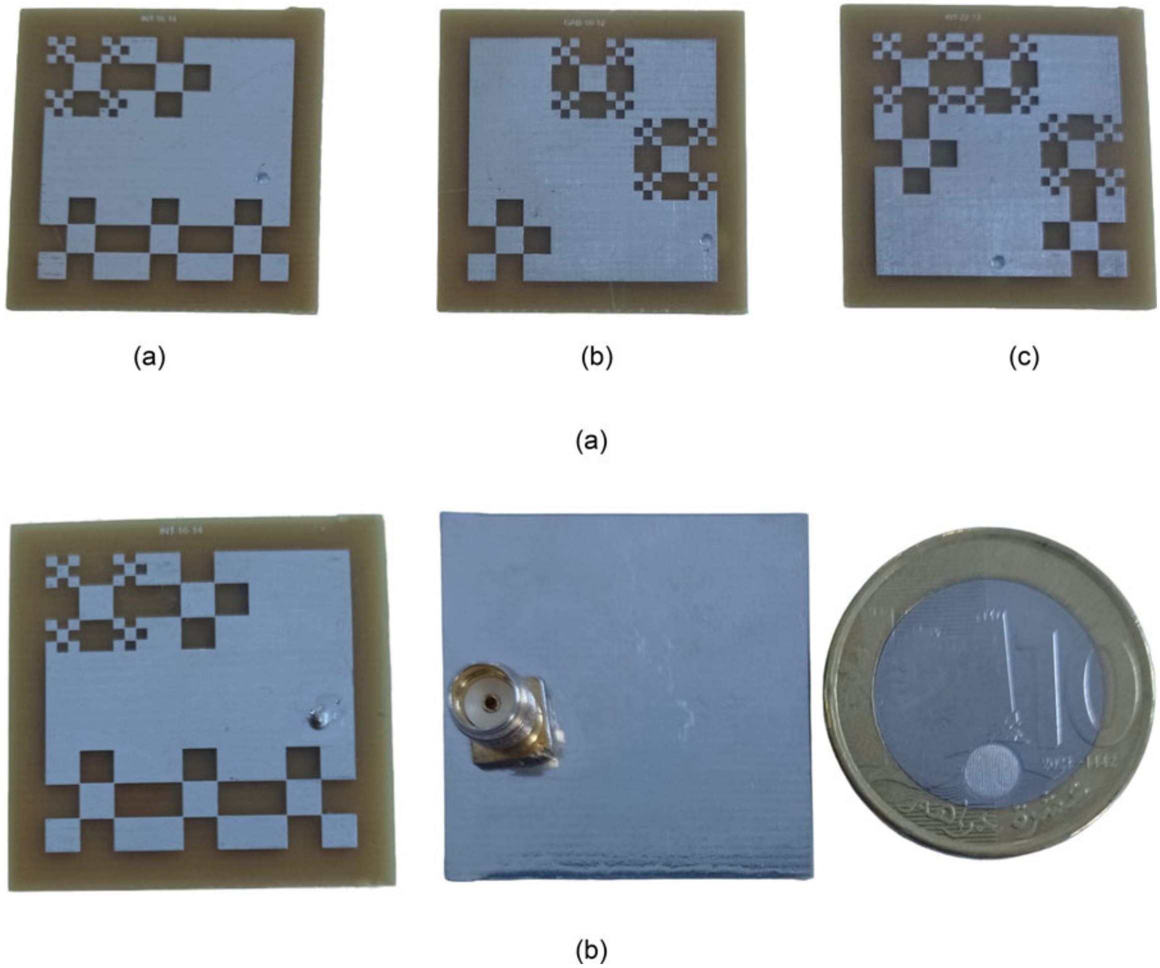

Figure 12. (a) Realized prototype antenna. (a) First, (b) second, (c) and third antenna. (b) Realized prototype antenna with the coax probe.

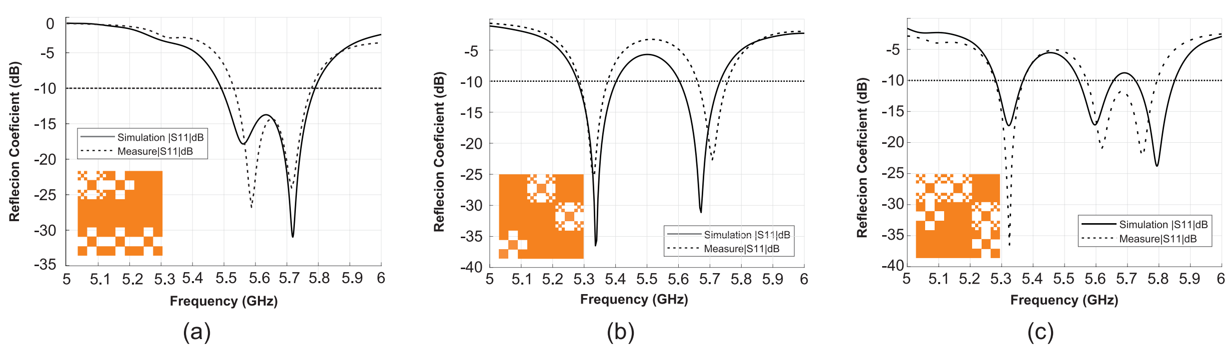

Figure 13. Simulated vs measured reflection coefficient of the (a) first, (b) second, (c) and third antenna.

Table 5. Summary of the realized bands and occupied channels for the three designed antennas

Antenna	Targeted WLAN band	Realized bands(GHz)	Realized/Target (%)	Occupied channels	Total channels
First(Wide band)	UNI–2C: 5.470–5.725	5.490–5.780	92	11/12	11
Second(Narrow Bi-band)	UNII–2A: 5.250–5.350	5.270–5.370	80	3/4	10
	UNII–2C: 5.470–5.725	5.590–5.730	53	7/12	
Third(Narrow Tri-band)	UNII–2A: 5.250–5.350	5.270–5.360	80	3/4	14
	UNII–2C: 5.470–5.725	5.530–5.650	50	6/12	
	UNII–3: 5.725–5.835	5.710–5.84	100	5/5	

https://doi.org/10.1017/S1759078723001071 Published online by Cambridge University Press

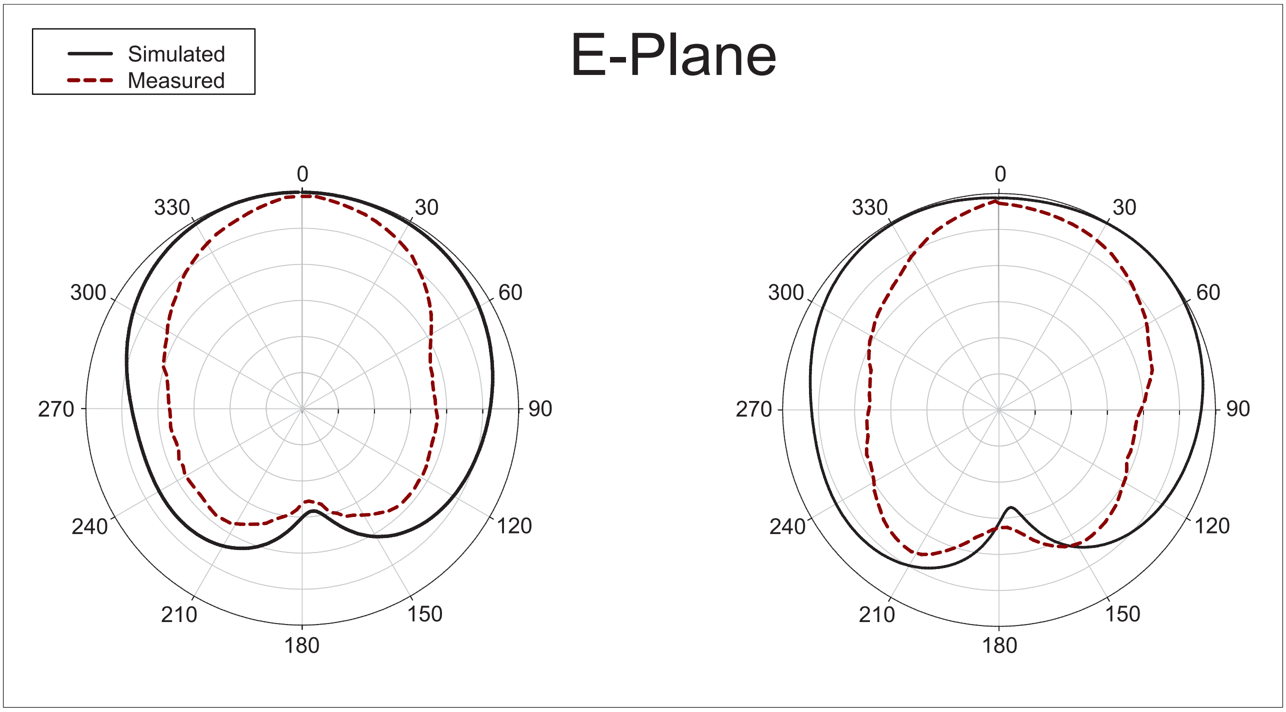

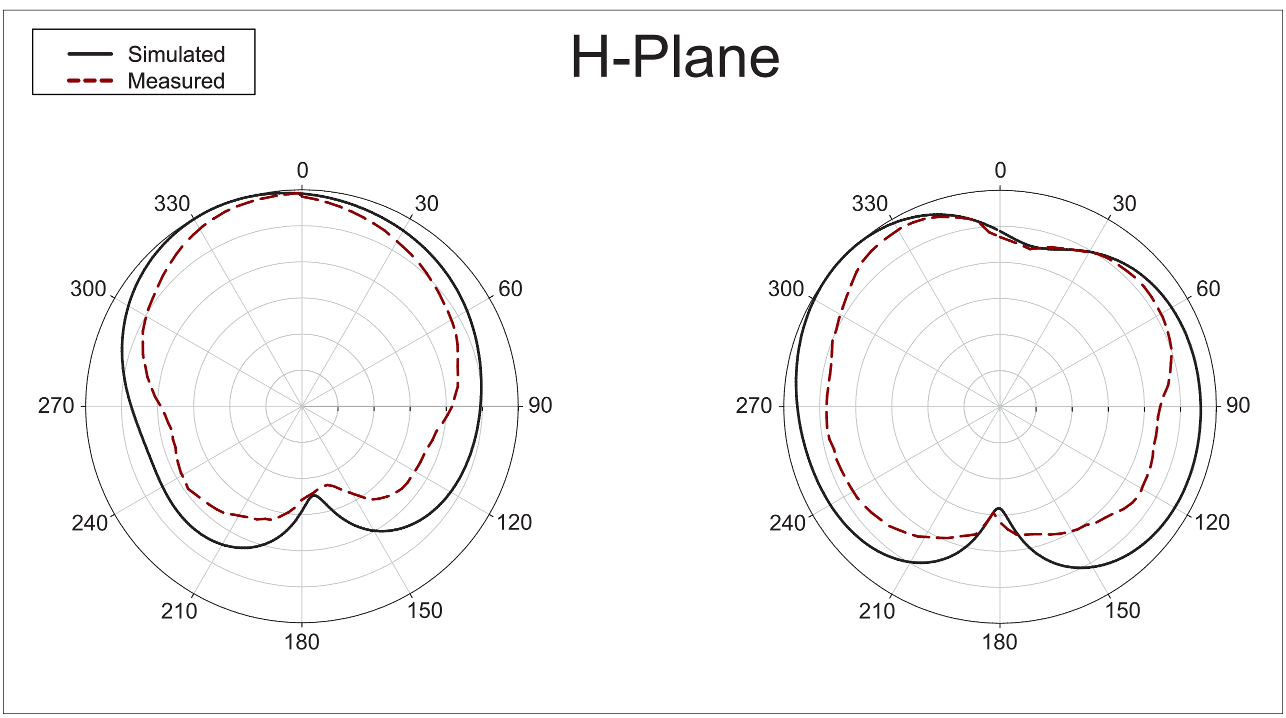

Figure 14. Simulated and measured 2D radiation patterns for the wide-band antenna at 5.56 GHz and 5.70 GHz.

time domain. This method remains very effective to avoid multiple parasitic reflections on walls and metal obstacles, and this is by an appropriate selection of delay and width of the measurement window.

Figures 14–16 show the measured 2D radiation patterns of the three designed antennas obtained in the E and H planes at different frequencies. Compared to the EM simulation results, a good agreement is obtained.

The methodology presented in this paper can quickly be adapted to other bands as needed by updating the fitness function. The GSM/UMTS/LTE bands can be added to replace the PIFA antennas widely used in mobile applications. PIFA antennas suffer from the problem that they are much thicker ($>$ 5 mm) in comparison to patch antennas ($<$ 1 mm) due to their multilayer aspect. In Table 6, the size and operating bands of the tri-band designed antenna are compared to some PIFA topologies.

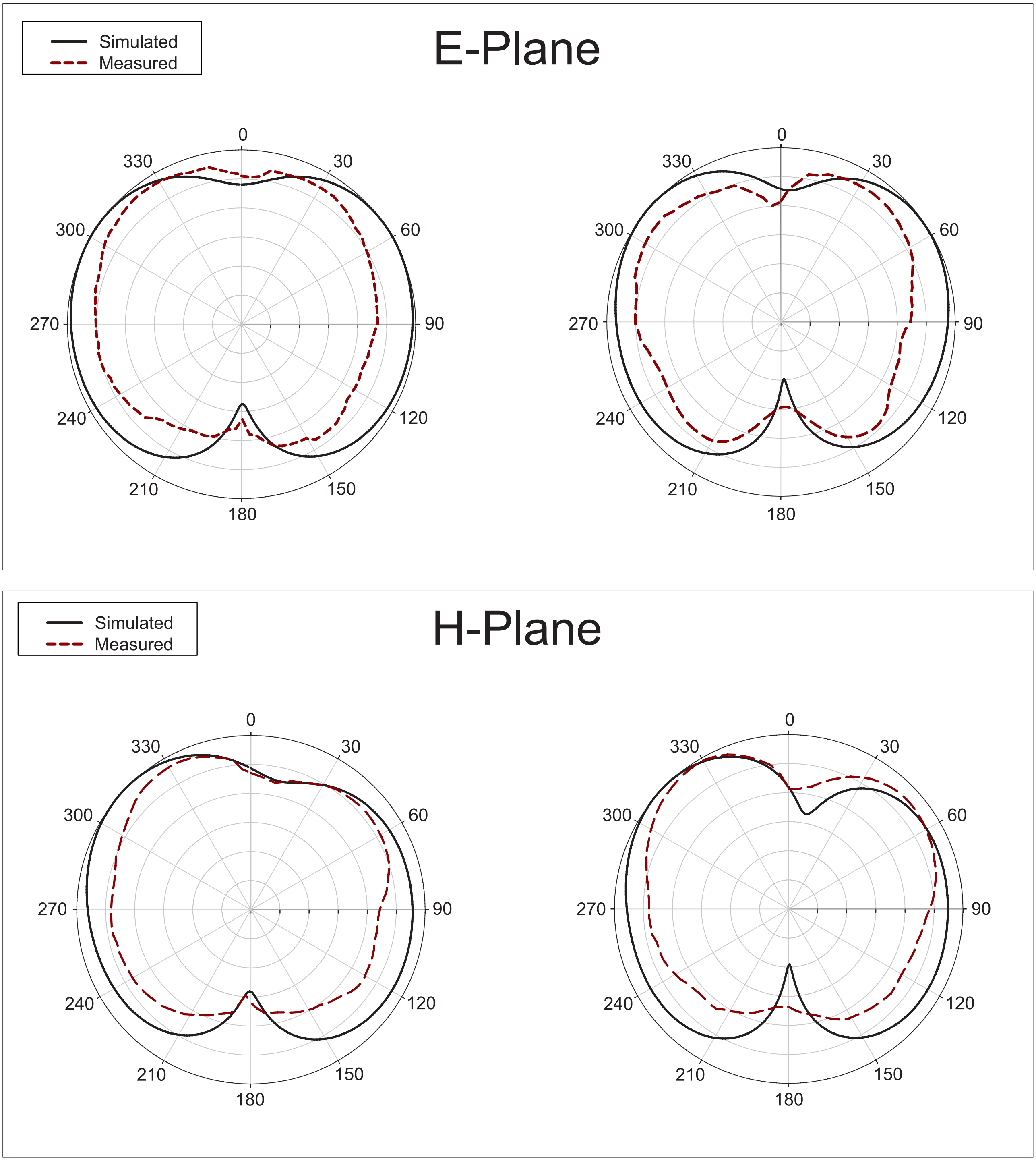

Figure 15. Simulated and measured radiation patterns for the dual-band antenna at both narrowband centers: 5.32 and 5.66 GHz.

The designed tri-band antenna is a $24 \times 24 \times 0.8$ mm^3 (460 mm^3) while the PIFA antenna presented in paper [26] is $30 \times 7 \times 5.8$ mm^3 (1218 mm^3) and $37 \times 24 \times 4$ mm^3 (3552 mm^3) for the PIFA presented in paper [27]. The methodology presented can then be very effective in terms of size reduction.

Conclusion

A GA with multi-objective fitness functions and parallel computing is applied to design three Minkowski Island fractal antennas for the WiFi-5 standard. The optimization process is accelerated by using the CST Application Programming Interface which allows all genetic operators to be performed in MATLAB while the numerical calculations are running the internal CST FDTD-solver using parallel computing and with GPU acceleration. This method allowed us to considerably reduce the convergence time. The whole process was then 9 times faster than normal. With single-objective GA-based optimization, a wideband antenna can be designed with high occupancy of the targeted band (92% for the first antenna). While the optimization based on the multi-objective

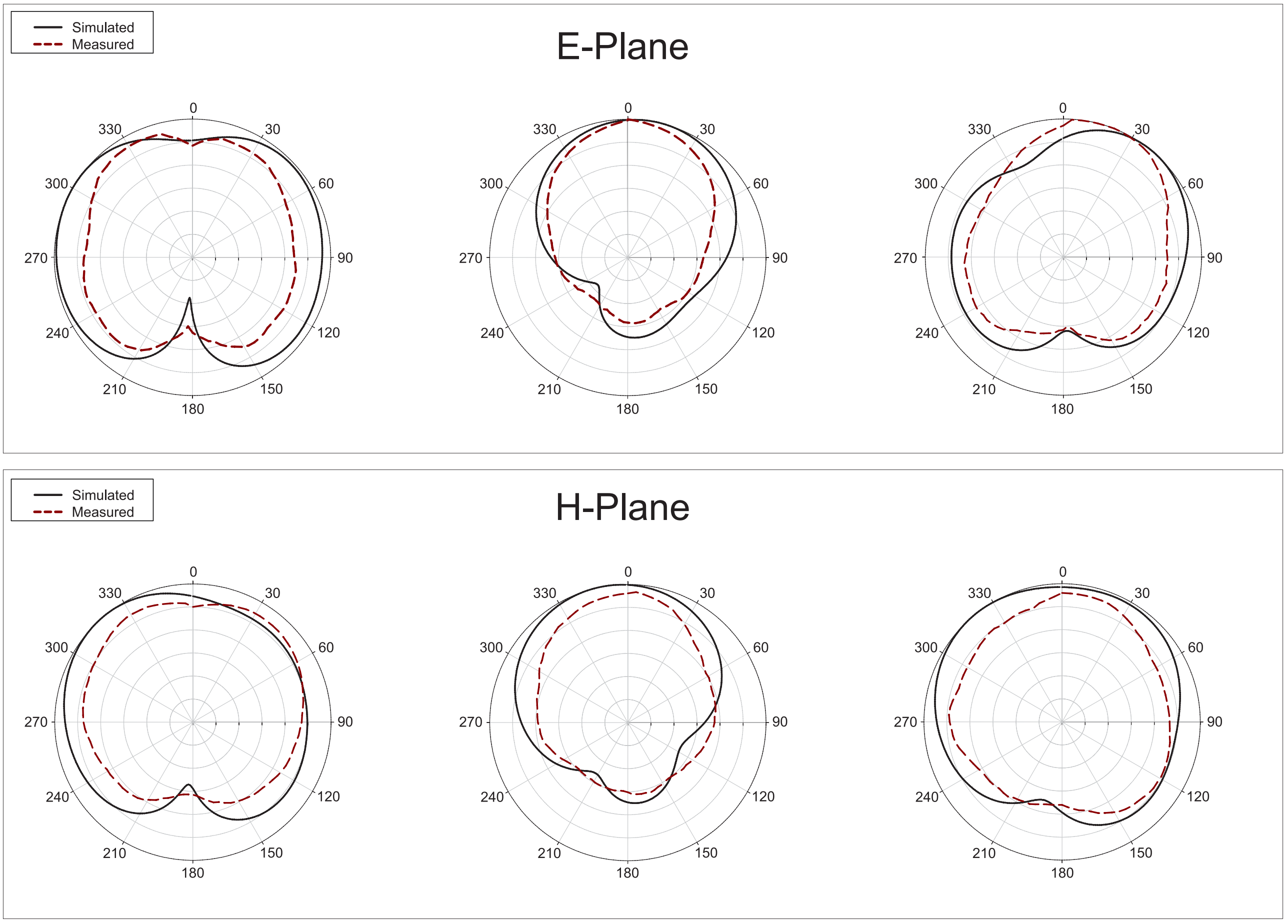

Figure 16. Simulated and measured radiation patterns for the tri-band antenna at the three narrowband centers: 5.32, 5.60, and 5.785 GHz.

Table 6. Performance comparison of this work to PIFA multiband antenna

Ref.	Topology	Size (mm^3)	Optimization method	Targeted bands
[26]	PIFA antenna	$30 \times 7 \times 5.8$	GA	Bluetooth/WLAN 2.4 GHz WLAN 5 GHz (UNII–1, UNII–2, UNII–3)
[27]	PIFA antenna	$37 \times 24 \times 4$	PSO	UMTS2100/LTE 2300/2600, Bluetooth/WLAN 2.4 GHz WLAN UNII–3
[28]	PIFA antenna	$30 \times 15 \times 5.4$	GA	LTE2600 WLAN (UNII–3) WiMAX
[29]	Fractal EBG and SRR	$40 \times 40 \times 1.6$	–	2.470 GHz 2.650 GHz
This work	Minkowski Island fractal	$24 \times 24 \times 0.8$	GA	UNII–2A: 5.250 — 5.350 GHz UNII–2C: 5.470 — 5.725 GHz UNII–3: 5.725 — 5.835 GHz

fitness function allows the designing of a multiband antenna with narrow bands and with many channels (14 channels for the braided band antenna).

Competing interests. The authors report no conflict of interest.

References

1. **Song Y, Jiao YC, Zhao G and Zhang FS** (2007) Multiband CPW-fed triangle-shaped monopole antenna for wireless applications. *Progress in Electromagnetics Research* **70**, 329–336.
2. **Cui Y, Yang L, Liu B and Li R** (2016) Multiband planar antenna for LTE/GSM/UMTS and WLAN/WiMAX handsets. *IET Microwaves, Antennas & Propagation* **10**(5), 502–506.
3. **Singh PP, Goswami PK, Sharma SK and Goswami G** (2020) Frequency reconfigurable multiband antenna for IoT applications in WLAN, Wi-Max, and C-band. *Progress in Electromagnetics Research C* **102**, 149–162.
4. **Gao SS, Luo Q and Zhu F** (2014) *Circularly Polarized Antennas*. Chichester: John Wiley & Sons.
5. **Byndas A, Hossa R, Bialkowski ME and Kabacik P** (2007) Investigations into operation of single-and multi-layer configurations of planar inverted-F antenna. *IEEE Antennas and Propagation Magazine* **49**(4), 22–33.
6. **Fernandes EMF, da Silva MW, da Silva Briggs L, de Siqueira Campos AL, de Araújo HX, Casella IR, Capovilla CE, Souza VP and de Matos LJ** (2019) 2.4–5.8 GHz dual-band patch antenna with FSS reflector for radiation parameters enhancement. *AEU-International Journal of Electronics and Communications* **108**, 235–241.
7. **Christydass SPJ and Gunavathi N** (2021) Octa-band metamaterial inspired multiband monopole antenna for wireless application. *Progress in Electromagnetics Research C* **113**, 97–110.

8. **Rajkumar R and Usha Kiran K** (2016) A compact metamaterial multiband antenna for WLAN/WiMAX/ITU band applications. *AEU-International Journal of Electronics and Communications* **70**(5), 599–604.
9. **Karmakar A** (2021) Fractal antennas and arrays: A review and recent developments. *International Journal of Microwave and Wireless Technologies* **13**(2), 173–197.
10. **Bhatia SS and Singh Sivia J** (2019) On the design of fractal antenna array for multiband applications. *Journal of the Institution of Engineers (India): Series B* **100**(5), 471–476.
11. **Liu G, Liang X and Zhensen W** (2013) Dual-band microstrip RFID antenna with tree-like fractal structure. *IEEE Antennas and Wireless Propagation Letters* **12**, 976–978.
12. **Yadav K, Jain A, Osman Sid Ahmed NM, Saad Hamad SA, Dhiman G and Alotaibi SD** (2022) Internet of thing based Koch fractal curve fractal antennas for wireless applications. *IETE Journal of Research*, 1–10.
13. **Rengasamy R, Dhanasekaran D, Chakraborty C and Ponnan S** (2021) Modified Minkowski fractal multiband antenna with circular-shaped split-ring resonator for wireless applications. *Measurement* **182**, 109766.
14. **Alibakhshi-Kenari M, Naser-Moghadasi M, Ali Sadeghzadeh R, Virdee BS and Limiti E** (2016) Dual-band RFID tag antenna based on the Hilbert-curve fractal for HF and UHF applications. *IET Circuits, Devices & Systems* **10**(2), 140–146.
15. **Sivasundarapandian S and Suriyakala CD** (2017) A planar multiband Koch snowflake fractal antenna for cognitive radio. *International Journal of Microwave and Wireless Technologies* **9**(2), 335–339.
16. **Moradi-Pari E** (2019) 5.9 GHz spectrum sharing. In Miucic R (ed), *Connected Vehicles*. Cham: Springer, 203–216.
17. **Haupt RL and Ellen Haupt S** (2004) *Practical Genetic Algorithms*. Hoboken: John Wiley & Sons.
18. **Gulati M, Siddharth S, Vedi Y and Susila M** (2018) Genetic-algorithm based planar antenna design. In *2018 International Conference on Wireless Communications, Signal Processing and Networking (WiSPNET)*, Chennai, India, pp. 1–2.
19. **Lamsalli M, El Hamichi A, Boussouis M, Touhami NA and Elhamadi T** (2016) Genetic algorithm optimization for microstrip patch antenna miniaturization. *Progress In Electromagnetics Research Letters* **60**, 113–120.
20. **Kanni VR and Brinda R** (2019) Design of high gain microstrip antenna for vehicle to vehicle communication using genetic algorithm. *Progress in Electromagnetics Research M* **81**, 167–179.
21. **Jayasinghe JW** (2021) Application of genetic algorithm for binary optimization of microstrip antennas: A review. *AIMS Electronics and Electrical Engineering* **5**(4), 315–333.
22. **Pérez-Moroyoqui R, Rodríguez-Romo S and Ibáñez-Orozco O** (2022) Genetic algorithm for the design of a multiband microstrip antenna with self-avoiding geometry obtained by backtracking. *International Journal of Communication Systems* **35**(18), e5345.
23. **Villegas FJ, Cwik T, Rahmat-Samii Y and Manteghi M** (2004) A parallel electromagnetic genetic-algorithm optimization (EGO) application for patch antenna design. *IEEE Transactions on Antennas and Propagation* **52**(9), 2424–2435.
24. **Chen Y, Zhang Y, Lin Z, Zhao X and Jiang S** (2014) GPU accelerated parallel MoM for simulating microstrip antenna array. In *Proceedings of 2014 3rd Asia-Pacific Conference on Antennas and Propagation*. IEEE.
25. **Liu J-C, Liu HH, Yeh KD, Liu CY, Zeng BH and Chen CC** (2012) Miniaturized dual-mode resonators with Minkowski-island-based fractal patch for WLAN dual-band systems. *Progress in Electromagnetics Research C* **26**, 229–243.
26. **Jayasinghe JM and Uduwawala D** (2015) A novel multiband miniature planar inverted F antenna design for bluetooth and WLAN applications. *International Journal of Antennas and Propagation* **2015**, 1–6.
27. **Wakrim L, Ibnyaich S and Hassani MM** (2017) Multiband operation and performance enhancement of the PIFA antenna by using particle swarm optimization and overlapping method. *Applied Computational Intelligence and Soft Computing* **2017**, 1–8.
28. **Wakrim L, Yassini AE, Khabba A, Ibnyaich S and Hassani MMR** (2021) Novel design of a triple band PIFA antenna by using a binary genetic algorithm. *Journal of Computational Electronics* **20**(3), 1373–1386.
29. **Sedghi MS, Naser-Moghadasi M and Zarrabi FB** (2017) Microstrip antenna miniaturization with fractal EBG and SRR loads for linear and circular polarizations. *International Journal of Microwave and Wireless Technologies* **9**(4), 891–901.

Bouchra Ezzahry was born in Fnideq, Morocco, in 1991. She received her License degree in 2013. She obtained her master's degree in Electronics and Telecommunications in 2015 from the Abdelmalek Essaadi University Tetouan, Morocco. She follows her research in the laboratory of information systems and telecommunications. She is currently pursuing her Ph.D. research in the field of optimization of fractal microstrip antennas using the genetic algorithm (GA).

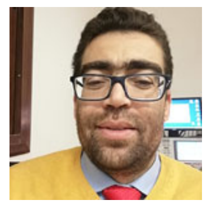

Tajeddin Elhamadi was born in Alhoceima, Morocco, in 1982. He obtained his master's degree in Electronics and Telecommunications in 2013 from Abdelmalek Essaadi University. In 2017, he obtained his Ph.D. degree in Physics from Abdelmalek Essaadi University, Tetouan, Morocco. Currently, Elhamadi is a researcher at the Faculty of Sciences at Abdelmalek Essaadi University. He directs his research in the information systems and telecommunications laboratory. His research work focuses on the characterization and modeling of microwave devices using neural networks, as well as the design of microwave circuits in GaAs and GaN MMIC technology. His research interests also include the optimization of planar circuits using evolutionary algorithms. In particular, the optimization of planar antennas by the genetic algorithm and the particle swarm optimization algorithm. Recently, he was introduced to the field of artificial intelligence and machine learning and their applications in the field of robotics and self-driving.

Mohammed Lamsalli was born in Kenitra, Morocco, in 1980. He received his bachelor's degree in 2006 from the Univ. Ibn Tofail (Science FS – Kenitra). In 2010, he took his master's degree from the University Abdelmalek Essaâdi (Science FS – Tetouan). He completed his Ph.D. in 2019 at Abdelmalek Essaadi University (Faculty of Sciences – Tetouan) in the field of electronics and telecommunications. His research focused on optimizing passive and active structures through the utilization of genetic algorithms. He received DESA in Instrumentation and Electronics and Ph.D. degree in Electronics and Telecommunication from the University of Abdelmalek Essaadi in 2002 and 2009, respectively. He received the AECID scholarship from the Spanish Ministry of Foreign Affairs (2005–2008) and participated in several research projects. He is an associate professor of electronics and telecommunications at the University of Abdelmalek Essaadi and a member of EIRT.

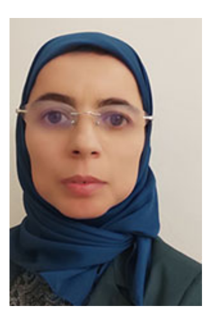

Naima Amar Touhami received DESA in Instrumentation and Electronics and Ph.D. degree in Electronics and Telecommunication from the University of Abdelmalek Essaadi in 2002 and 2009, respectively. She received the AECID scholarship from the Spanish Ministry of Foreign Affairs (2005–2008) and participated in several research projects. She is an associate professor of electronics and telecommunications at the University of Abdelmalek Essaadi and a member of EIRT. She has supervised master's and bachelor's degree students. She has more than 40 journal papers and 40 conference papers. She has participated in the organization of some conferences and events for Ph.D. students. Her research interests include synthesis of advanced high-performance active and passive circuits such as antennas, filters, diplexer, amplifier, and mixer.

https://doi.org/10.1017/S1759078723001071 Published online by Cambridge University Press